

Predicting Harmful Algal Blooms and Impacts on Shellfish Mariculture using Novel Data-Driven Approaches

Oliver Stoner

University of Glasgow <https://orcid.org/0000-0003-0612-4306>

Theo Economou

University of Exeter

Ricardo Torres

Plymouth Marine Laboratory

Ian Ashton

University of Exeter

Andrew Brown (✉ ross.brown@exeter.ac.uk)

University of Exeter

Article

Keywords: Phycotoxin Concentrations, Dinophysis Species, Spatiotemporal Statistical Modelling Framework, Optimal Siting, Safe Harvesting Periods

Posted Date: July 15th, 2021

DOI: <https://doi.org/10.21203/rs.3.rs-668820/v1>

License:  This work is licensed under a Creative Commons Attribution 4.0 International License.

[Read Full License](#)

Predicting Harmful Algal Blooms and Impacts on Shellfish Mariculture using Novel Data-Driven Approaches

Oliver Stoner¹, Theo Economou², Ricardo Torres³, Ian Ashton⁴, A Ross Brown⁵

¹School of Mathematics and Statistics, University of Glasgow, UK; ²Department of Mathematics, University of Exeter, UK;

³Plymouth Marine Laboratory, Prospect Place, Plymouth, UK; ⁴Department of Engineering, University of Exeter, UK;

⁵Department of Biosciences, University of Exeter, UK.

Address correspondence to ross.brown@exeter.ac.uk

Harmful algal blooms (HABs) intoxicate and asphyxiate marine life, causing devastating environmental and socio-economic impacts costing at least \$8bn/yr globally. Accumulation of phycotoxins from HAB phytoplankton in filter-feeding shellfish can poison human consumers, prompting site harvesting closures if concentrations in shellfish exceed safe levels. To better quantify both long- and short-term HAB risks, we developed novel data-driven approaches to predict phycotoxin concentrations in bivalve shellfish associated with HAB forming *Dinophysis* species. Our spatiotemporal statistical modelling framework assesses long-term HAB risks for different shellfish species in both data-rich and data-poor locations. This can revolutionise mariculture management by more confidently informing optimal siting of new shellfish operations and safe harvesting periods for businesses. Meanwhile, our machine learning framework forecasts phycotoxin concentrations further into the future than previously possible. Across 6 coastal, estuarine and loch sites, we achieve 87% overall accuracy in predicting future harvesting shutdowns 0-8 weeks ahead.

Aquaculture will play a key role in future food security. Global aquaculture production has recently overtaken capture fisheries by producing 82 million tonnes of food fish per year globally (worth US\$232 billion), with projections rising to 109 million tonnes by 2030¹. Marine aquaculture (mariculture) shows enormous potential for sustainable food production². Expanding the farming of marine bivalve shellfish (currently amounting to 17.3 million tonnes, worth over \$24 billion per year globally) is particularly attractive, since these filter feeders derive their food from freely available marine planktonic microalgae; shellfish also perform a wide range of ecosystem services, including nutrient regulation and carbon capture^{1,3}.

However, future expansion of bivalve mariculture depends on several socio-economic and environmental constraints relating to competing demands from other marine economic activities⁴, environmental carrying capacities⁵ and environmental hazards, including adverse climatic conditions, pollution, and Harmful Algal Blooms (HABs)⁶. The increasingly frequent and widespread occurrence of HABs, proliferations of harmful planktonic algae causing intoxication and/or asphyxiation of marine life, is a major constraint on bivalve shellfish mariculture in NW European

46 shelf seas and other HAB hotspots around the globe⁷⁻¹⁰. Global annual economic
47 impacts of HABs exceed \$8 billion, approximately half due to enforced seafood
48 harvesting bans or product recalls and half due to unavoided HAB toxin-related
49 human health costs^{11,12}. In NW Europe, dinoflagellate HAB species from the genus
50 *Dinophysis* (*Dinophysis acuminata* and *Dinophysis acuta*) are particularly
51 problematic, since low biomass blooms of these species >100 cells/L are sufficient to
52 intoxicate bivalves and cause diarrhetic shellfish poisoning in human consumers^{13,14}.
53 These low biomass blooms are undetectable by satellite surveillance and, as with
54 several other dinoflagellate HAB species, they are likely to increase in prevalence
55 with global warming, thermal stratification, and stabilisation of the water
56 column^{7,9,15,16}.

57
58 There is an immediate need for new tools to better quantify long-term and short-term
59 changes in HAB risk, to design optimal mitigation strategies. Contemporaneous HAB
60 surveillance, including for *Dinophysis* spp., relies on regular weekly or bi-weekly *in*
61 *situ* sampling and subsequent chemical analysis of phycotoxins in shellfish,
62 alongside microscopic quantification of HAB species abundance at routine
63 monitoring points across regulatory networks e.g. in the UK and EU¹⁷. Meanwhile,
64 predicting HAB events is highly complex, due to multiple environmental drivers
65 varying temporally from seconds to decades; and spatially, from the microscopic
66 scale (mm) to the mesoscale (100 km). These include physical factors driving water
67 stratification and nutrient depletion, as well as mixing and nutrient replenishment.
68 Ecological interactions between HAB species, other planktonic organisms and their
69 physico-chemical environments can also be highly influential, notably resource
70 competition, predation, and parasitism – which can invoke biochemical (allelopathic)
71 defence mechanisms involving phycotoxins^{10,18}. Phycotoxins, including *Dinophysis*
72 toxins (Okadaic Acid (OA), *Dinophysis* toxin (DTX), Pectenotoxin (PTX)), are heat
73 stable and not affected by cooking, which contribute to their risk to human health¹³.

74
75 Existing HAB models account for spatial and temporal variation either: explicitly in
76 the case of dispersion models¹⁹ (Davidson et al., 2016) and mechanistic models
77 incorporating key ecological life-history processes²⁰, or implicitly in the case of data
78 models (i.e. statistical or machine learning models) that incorporate short-term and
79 long-term trends^{19,21}. Data models are simpler and less subject to structural errors at
80 the expense of overlooking mechanistic/process detail. Moreover, coupled with
81 probabilistic elements, data models can quantify the uncertainty associated with any
82 estimates or predictions. Provided they are updated regularly (with new data), data
83 models can be developed for generating short-term predictions²², with the potential
84 to inform short-term operational planning decisions for mariculture businesses¹⁰.
85 Recent approaches have been shown to have increasing skill in making more
86 reliable short-term predictions, notably via increasingly sophisticated smoothing
87 functions²³ or threshold functions accounting for sudden shifts, e.g. when
88 temperature falls below tolerable or optimal physiological limits for a HAB species²⁴.
89 Until now, accurate HAB forecasting has generally been limited to 1-2 weeks,
90 corresponding to the general extent and accuracy of meteorological
91 forecasting^{19,23,25,26}. These existing approaches, which mostly utilise meteorological
92 and hydrographical variables as predictors, tend to 'over-predict' HAB duration¹⁹.

93 While reassuring for human safety, this is not so appealing to businesses waiting for
94 harvesting bans to be lifted⁶.

95

96 Here we present novel data modelling approaches to quantify HAB risk from
97 *Dinophysis* spp., based on 10-20 years of Official Control monitoring data for a range
98 of shellfish species at coastal sites around Scotland, SW England, and Northern
99 France. We leverage the direct connection between these data and regulatory action
100 levels for *Dinophysis* toxins (i.e. 160 µg/kg Okadaic Acid equivalents [OA eq.] in
101 shellfish flesh) to better understand impacts on shellfish mariculture. To quantify
102 long-term HAB risks, we present a statistical framework built on advanced smoothing
103 techniques capable of evaluating spatiotemporal trends in average *Dinophysis* toxin
104 concentrations in shellfish. Then, we present a machine learning approach combined
105 with statistical pre- and post-processing to forecast toxin concentrations in shellfish
106 up to 8 weeks into the future.

107 1 Long-term risk assessment and spatial planning

108

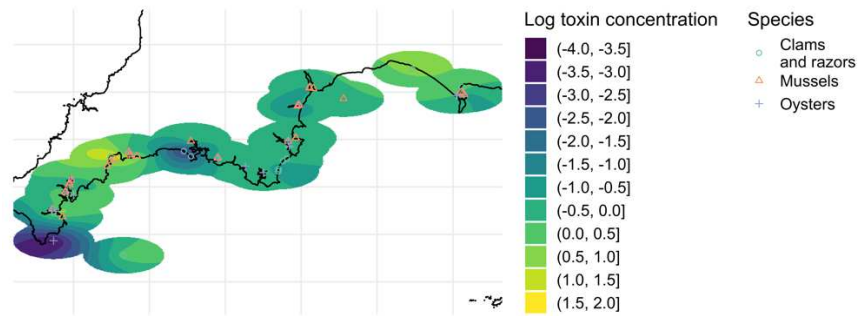
109 Using advanced smoothing methods based on penalised regression splines²⁷, we
110 developed data models implemented on data from individual study regions
111 incorporating medium- to long-term temporal (seasonal and interannual), spatial, and
112 shellfish species-specific variability in *Dinophysis* toxin concentrations. The models
113 can capture structured interactions between spatial and temporal variability in toxin
114 concentration to quantify HAB risk in new and data poor sites, while also quantifying
115 the relative susceptibility of different shellfish species for accumulating *Dinophysis*
116 toxins within each national dataset. The models can therefore aid site selection
117 through spatial estimates of toxins (Section 1.1), harvest planning through
118 spatiotemporal estimates of toxins (Section 1.2) and species selection for different
119 sites (Section 1.3).

120

121 1.1 Overall spatial distribution of *Dinophysis* toxins

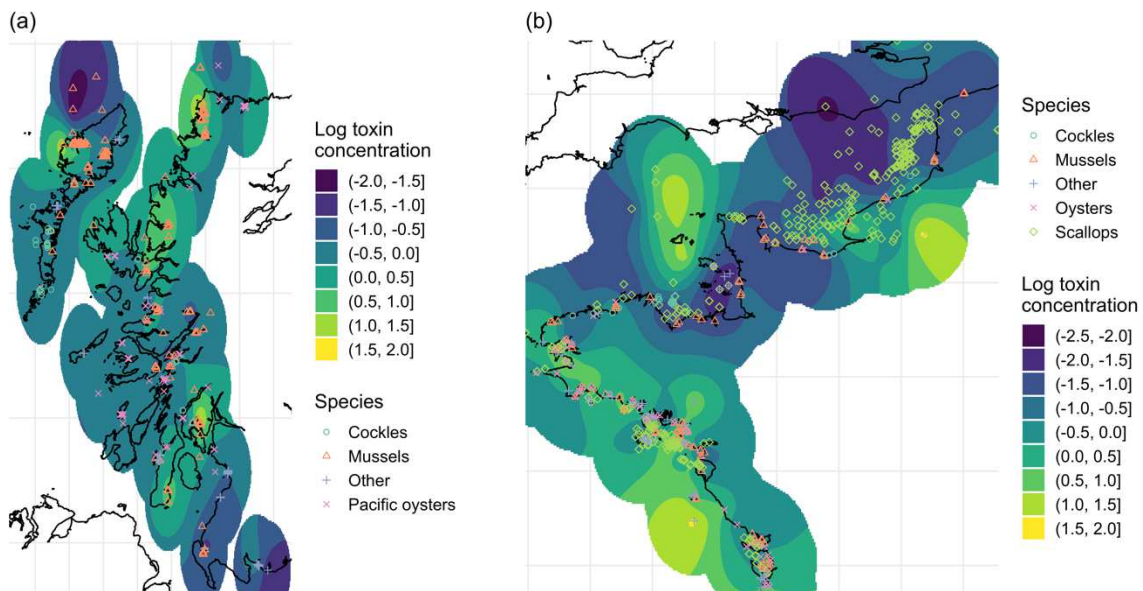
122 Estimates of long-term average HAB toxicity can be used to indicate persistent or
123 frequently recurring blooms and can therefore inform decisions about suitable
124 locations for shellfish farming. Here we show the estimated effect of location on
125 average *Dinophysis* toxin concentrations in shellfish (at the log-scale, e.g. a location
126 with a plotted value of 2 has an $\exp(2) \approx 7.4$ times higher average toxin
127 concentration than a location with a plotted value of 0), for South-West England
128 (Figure 1), Scotland (Figure 2a) and France (Figure 2b).

129



130
131
132 Figure 1: Estimated spatial variation in log *Dinophysis* toxin concentrations in South-West England. Symbols indicate location of shellfish sites and species monitored for *Dinophysis* toxins.

133 In SW England (Figure 1), *Dinophysis* HAB hotspots (highlighted in yellow) include
134 Lyme Bay to the east and Falmouth Bay and St Austell Bay to the west. The western
135 areas are particularly at risk, since they are sheltered to some extent from prevailing
136 SW winds and undergo rapid sea surface warming and prolonged thermal
137 stratification during the summer^{28,29}.
138



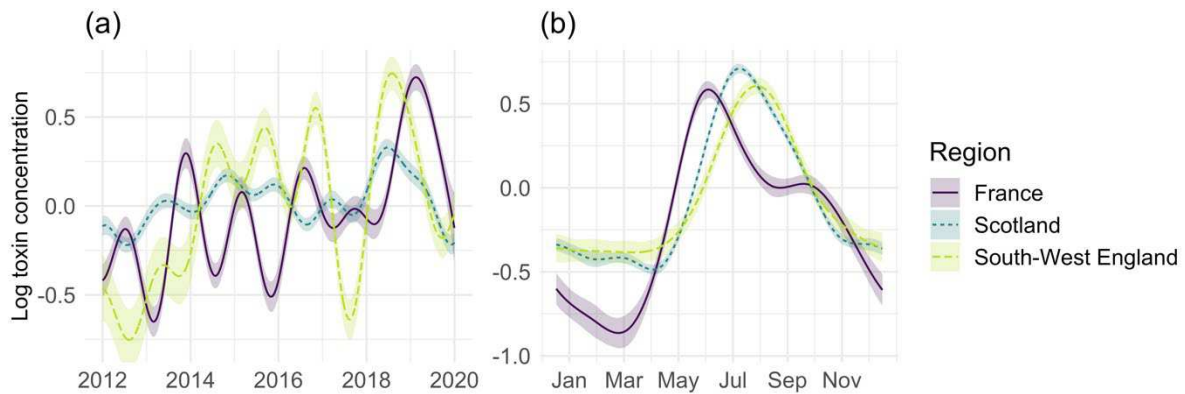
139
140
141
142 Figure 2: Estimated spatial variation in log *Dinophysis* toxin concentrations in (a) the West coast of Scotland and (b) the north and west coasts of France. Symbols indicate location of shellfish sites and species monitored for *Dinophysis* toxins.

143 The majority of Scottish shellfish sites (Figure 2a) are located on Scotland's west
144 coast, and mainly harvest blue mussels (*Mytilus edulis*) and cockles (*Cerastoderma*
145 *edule*). These sites are warmed by the North Atlantic Current, extending from the
146 Gulf Stream. Regularly recurring HAB hotspots are in the relatively sheltered Clyde
147 Sea and along the indented NW coast.
148

149 Shellfish production sites in France are depicted for the north and west coasts
150 (Figure 2b); HAB hotspots comprise wild beds, including offshore king scallop
151 (*Pecten maximus*) beds in the English Channel, as well as embayments along the
152 north and west coast containing wild and cultivated scallops, Pacific oysters and blue
153 mussels.
154

155 **1.2 Seasonal variation in *Dinophysis* toxin concentrations**

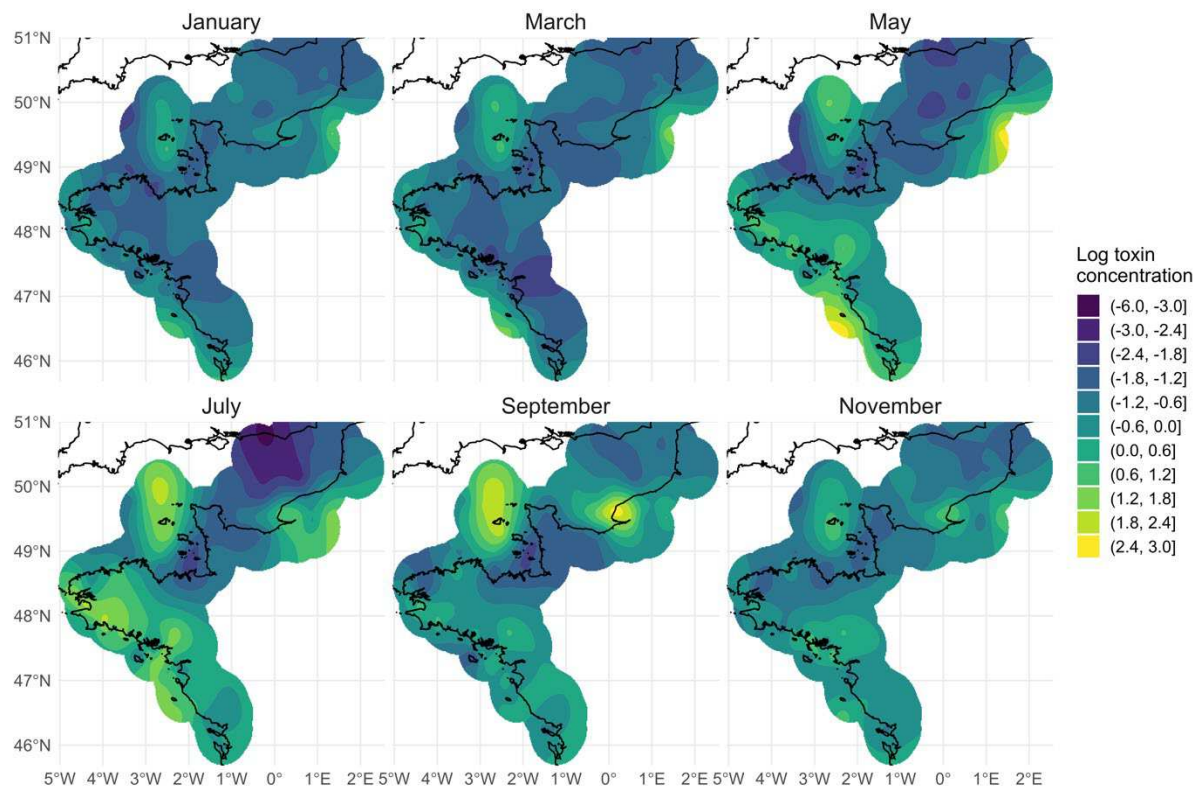
156 A clear understanding of systematic seasonal variability, or in other words what we
157 expect the average toxin levels in shellfish to be at different times of the year, is
158 essential for developing a sustainable maricultural industry, i.e. for site selection and
159 mitigation of HAB impacts through optimal harvest scheduling (whilst also accounting
160 for market conditions). Our models for France, Scotland and South-West England
161 estimate overall temporal and seasonal signals in *Dinophysis* toxin concentrations at
162 a national level, as illustrated in Figure 3.
163



164
165 *Figure 3: Estimated (a) temporal and (b) seasonal signals in the mean (log) toxin concentration for each study*
166 *region (from the spatial/main effects model), with 95% confidence intervals.*

167 In SW England, toxin concentrations indicated an increasing trend over the last
168 decade (most visible in the peaks), interrupted temporarily in 2017, when
169 concentrations fell substantially (Figure 3a). Consecutive seasonal (summer) peak
170 toxin concentrations in SW England and Scotland corresponded closely in timing,
171 while toxin concentrations in France did not synchronise with them. Furthermore, in
172 France there was some evidence of a repeating pattern of a larger followed by a
173 smaller toxin spike in consecutive years. Nevertheless, maximum toxin
174 concentrations were recorded from all three data series in 2018, one of the warmest
175 summers on record in NW Europe³⁰.

176
177 The seasonally averaged signals for Scotland and SW England were similar,
178 displaying an approximately symmetrical shape with single peaks occurring around
179 July-August, while the highest toxin concentrations for France occur around June,
180 followed by a further small increase/inflection in the Autumn (Figure 3b). Examining
181 space-season interactions (Figure 4), our model showed that peak toxicity occurs in
182 July along France's Atlantic coast, while on the north coast the peak occurs later in
183 the summer and early autumn.
184

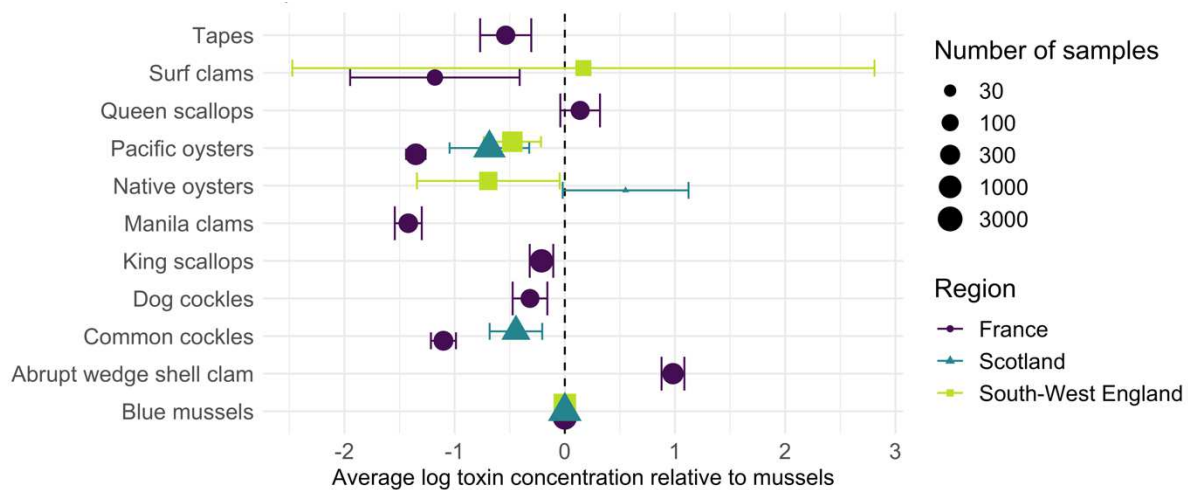


185
186
187

Figure 4: Estimated average (relative) toxin levels in France at different times of the year, from the spatiotemporal model for French *Dinophysis* toxin data.

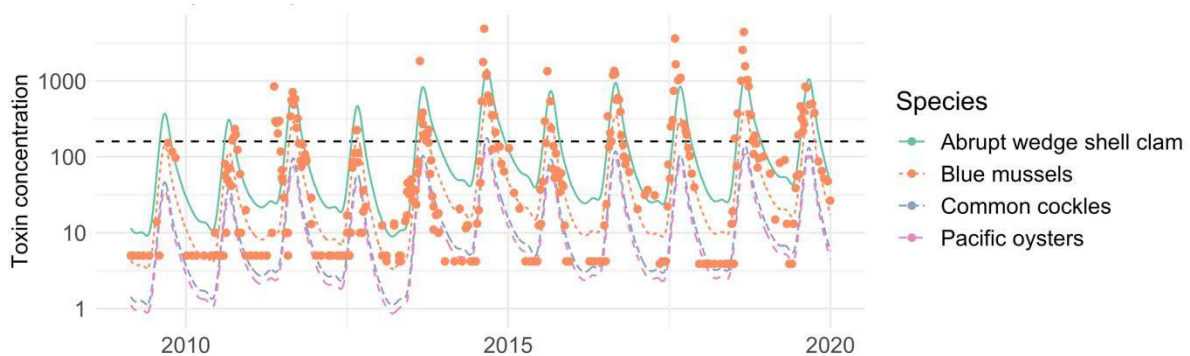
188 1.3 Vulnerability of shellfish species and spatial planning

189 Our models also estimated the average *Dinophysis* toxin concentrations for each
 190 study region in different shellfish species relative to the average toxin concentration
 191 in blue mussels (Figure 5). By considering both the point estimates and uncertainty
 192 (95% confidence intervals, shown as error bars), we can draw conclusions about the
 193 risks associated with the farming of different shellfish species. We only compared
 194 estimates for species with at least 200 data points in total across all regions. Several
 195 species exhibited similar average levels of intoxication to mussels, including Dog
 196 cockles, King scallops and Queen scallops. Meanwhile, Manila clams, Pacific
 197 oysters and common cockles in France exhibited substantially lower average toxin
 198 concentrations than blue mussels. Both native oysters in Scotland and abrupt wedge
 199 shell clams (*Donax trunculus*) in France exhibited substantially higher average toxin
 200 levels compared to mussels.
 201



202
 203
 204
 205
 206
 207
 Figure 5: Estimated species effect (variation in *Dinophysis* toxin concentrations across shellfish species) from the long-term spatial risk models for France, Scotland, and South-West England. Effects are shown relative to the point estimates for blue mussels (*Mytilus edulis*) for each region. Points show point estimates and error bars show 95% uncertainty intervals. The size of the point relates to the number of unique observations for each species, separately for each region.

208 Estimating the relative *Dinophysis* toxin concentrations for different shellfish species
 209 provides the opportunity to assess the potential change in HAB risk associated with
 210 the farming of alternative species at existing sites. For example, for Antifer ponton
 211 pêche on France's north coast, *Dinophysis* toxin concentrations in blue mussels,
 212 consistently exceeded the action level (160 $\mu\text{g}/\text{kg}$ OA eq., requiring harvesting
 213 closure) between 2010 and 2018, often for a month at a time (Figure 6). Our model
 214 suggests that, if it were possible for Pacific oysters or common cockles to be farmed
 215 here instead, the toxin concentration, and consequently the risk of disruption to
 216 harvesting, could be substantially reduced (Figure 6). Meanwhile, harvesting of
 217 abrupt wedge shell clams here could suffer from longer periods of enforced closure
 218 on average.
 219

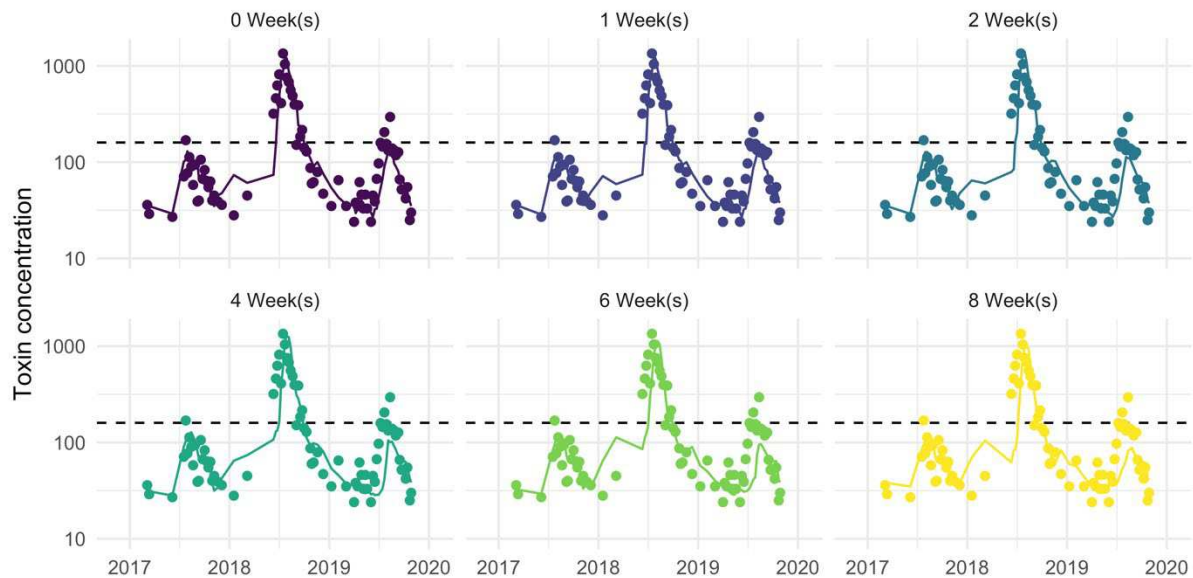


220
 221
 222
 223
 Figure 6: Estimated mean toxin concentration at **Antifer ponton pêche** for different species (lines). Points show the observed concentrations from blue mussel samples and the horizontal dashed line shows the toxin threshold above which harvesting is shut down.

224 2 Forecasting harvesting closures

225
 226 Using only short- to medium-term histories of sea surface temperature and
 227 *Dinophysis* abundance (cell counts in water), lagged at intervals of 0-12 weeks as
 228 inputs to a series of machine learning (random forest) models, we predicted future
 229 *Dinophysis* toxin concentrations for different forecasting lead times (0 to 8 weeks in
 230 the future). Models were trained for prediction at each of the following geographically

231 diverse sites in SW England: St Austell Bay (coastal); Fowey (Ria estuary); Lyme
232 Bay (offshore); and Scotland: Loch Eishort (inland sea loch); Loch Laxford (coastal
233 sea loch); and Sandsound Voe.
234



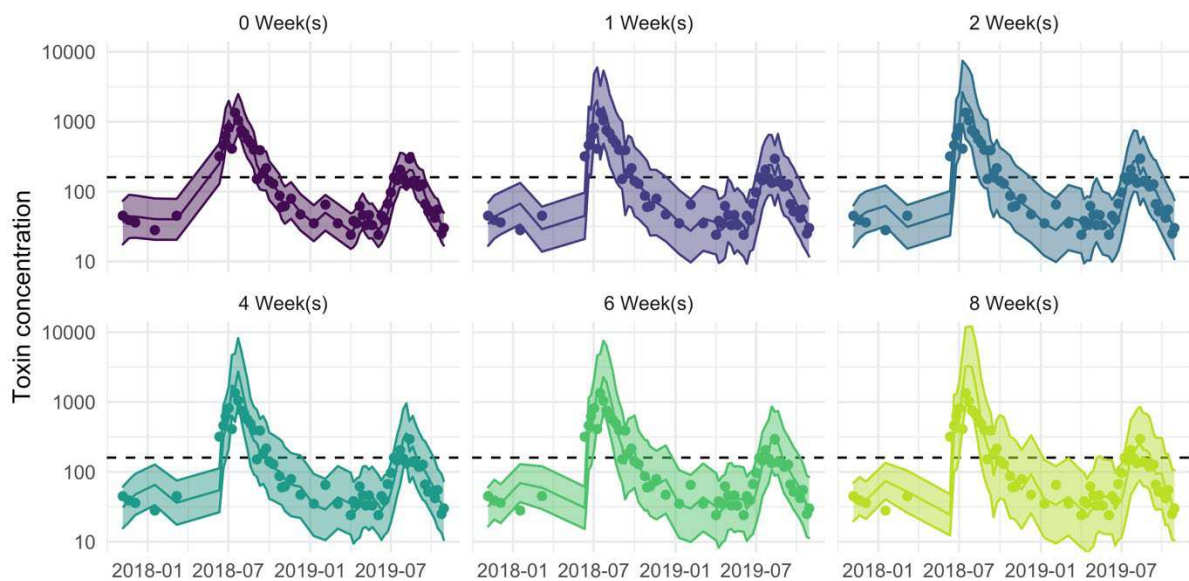
235
236
237
238
239
Figure 7: Predicted toxin concentrations from the machine learning algorithm (lines) for Sandsound Voe, where dots represent measured data. Each panel displays predictions from a specific forecasting lead time (e.g. 2 weeks). The horizontal dashed lines show the regulatory harvesting closure threshold (160 µg/kg OA equivalents).

240 Predicted *Dinophysis* toxin concentrations are plotted for Sandsound Voe, Shetland
241 Figure 7 over the 2018 and 2019 HAB seasons in Figure 7. In 2018, the measured
242 toxin concentration reached a peak of 1346 µg/kg OA eq in July and exceeded the
243 harvesting closure threshold for over 3 months. In contrast, the bloom in 2019 was
244 far less intense, reaching a peak of only 295 µg/kg OA eq in August. Similar plots
245 are available for other study sites in the Supporting Information. By combining the
246 information from the temperature and *Dinophysis* spp. abundance, the machine
247 learning algorithm can predict future patterns of *Dinophysis* toxin concentrations in
248 shellfish in relation to bloom parameters, including: i) the 'growth' versus 'decay'
249 phase for temperature and cell count; ii) bloom intensity versus threshold cell count
250 (trigger level = 100 cells/L) and versus threshold toxin concentration (action level =
251 160 µg/kg OA eq); and iii) seasonal trends. For all lead times, the models for
252 Sandsound Voe were able to capture the differences in intensities between the two
253 annual HAB events. Predictions of the toxin concentrations were particularly
254 impressive in 2018, with predictions closely matching the unknown future
255 observations, even when predicting 8 weeks into the future (Supplementary
256 Information).

257
258 However, some short-term discrepancies remained between predicted and observed
259 *Dinophysis* toxin concentrations. For example, the models for Sandsound Voe
260 systematically under-predicted the toxin level in the 2019 HAB season (Figure 7),
261 such that they failed to foresee a harvesting closure. Minimising these discrepancies
262 is vital to be able to accurately predict whether toxin concentrations will exceed or fall
263 short of the harvest closure threshold.
264

265 **2.1 Postprocessing and measures of uncertainty**

266 Figure 7A statistical “post-processing” algorithm was employed to obtain more
267 accurate predictions of *Dinophysis* toxin concentrations in shellfish. Specifically, we
268 fit a statistical model capturing systematic changes over time in the prediction errors
269 from the machine learning algorithm. Using this model, we predicted the error of a
270 new forecast and obtained a corrected prediction of intoxication. Finally, we
271 measured the uncertainty by computing the standard error of these corrected
272 predictions (see Supporting Information). Figure 8 shows the close concordance
273 between mean predicted (line) and measured (dots) log *Dinophysis* toxin
274 concentrations in blue mussels farmed in Sandsound Voe in NW Scotland.
275 Importantly, the under-prediction in 2019 was eliminated by the correction, such that
276 the risk of harvesting closure was then correctly identified. For this site, we also note
277 that the uncertainty in predictions increased marginally from 0 to 1 week but did not
278 sizeably increase from 1 to 8 weeks into the future.
279



280
281 *Figure 8: Corrected predictions of toxin concentrations in Sandsound Voe, obtained using the machine learning*
282 *algorithm and the statistical postprocessing algorithm, with each panel displaying predictions from a specific*
283 *forecasting lead time (e.g. 2 weeks). Upper/lower bounds are the corrected predictions plus/minus twice the*
284 *estimated standard error. The horizontal dashed lines show the regulatory harvesting closure threshold (160*
285 *µg/kg OA equivalents).*

286 **2.2 Accuracy and specificity of predictions**

287 We assessed the out-of-sample (nowcasting/forecasting) performance of the “raw”
288 predictions from the machine learning algorithm and the corrected predictions using
289 a suite of quantitative metrics. These are: the root mean-squared error (RMSE); R^2 ;
290 the true positive prediction rate (proportion of predictions which correctly identify the
291 toxin concentration as being greater than the harvesting closure threshold); and the
292 false positive prediction rate (proportion of predictions which incorrectly identify the
293 toxin concentration as being greater than the threshold).

294
295
296

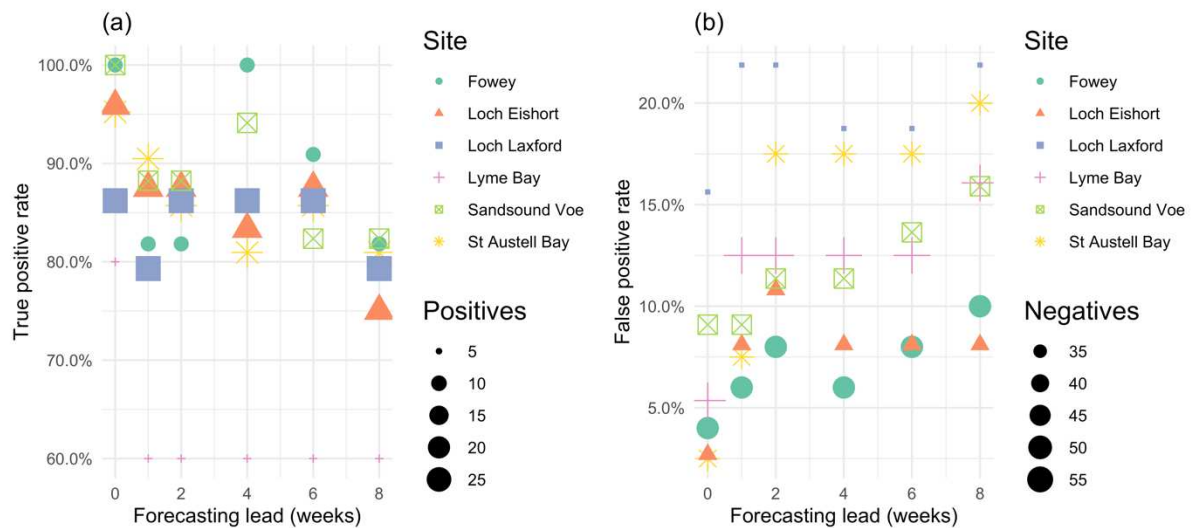


Figure 9: True positive prediction rate (a) and false positive prediction rate (b) (proportion of predictions which correctly/falsey identify the toxin concentration as being greater than the harvesting closure threshold). Diameter of symbol represents in (a) the number of threshold exceedances (positives) and in (b) the number of threshold deceedances (negatives).

297
298
299
300
301

302 For these study sites, excluding Lyme Bay where *Dinophysis* toxin concentrations
303 rarely exceeded harvesting thresholds, true positive prediction rates ranged from
304 about 80% to 100% when forecasting up to 6 weeks ahead, and from about 75% to
305 85% 8 weeks ahead (Figure 9a). The overall true positive rate for all sites and lead
306 time was 87%. Meanwhile, false positive prediction rates ranged from about 0% to
307 15% when nowcasting and about 5% to 20% when forecasting up to 8 weeks ahead
308 (Figure 9b).

309 3 Discussion

310

311 3.1 A step change in HAB risk assessment and forecasting

312 Better quantifying and predicting the risk of HABs is vital for sustaining the future
313 operation and growth of shellfish mariculture. Addressing a need for more advanced
314 risk assessment tools, we have developed novel data-driven approaches to exploit
315 standardised HAB monitoring data for shellfish production. Models based on our
316 proposed frameworks could be deployed to benefit HAB and biotoxin alert systems
317 in Scotland²⁶, SW England, Northern France and elsewhere in Northern Europe,
318 including Spain and Portugal and other key shellfish harvesting areas in the Atlantic
319 ARC and Mediterranean, which are plagued by *Dinophysis* HABs.

320

321 Using advanced multidimensional smoothing structures available within the
322 Generalized Additive Model framework, we have developed models which explicitly
323 account for spatiotemporal variability and interactions (e.g. space-season) in
324 *Dinophysis* toxin concentrations in shellfish. These models can predict average
325 annual HAB toxin risk profiles at new and data-poor sites, for a variety of shellfish
326 species, offering the potential to revolutionise marine spatial planning by identifying:
327 a) recurring HAB hotspots versus lower risk areas and b) opportunities for
328 optimisation of existing mariculture, through changes in farmed shellfish species
329 (informed by the weight of evidence across regions) and seasonal harvesting
330 schedules. For example, the French dataset showed earlier onset of *Dinophysis*
331 blooms and elevated toxin levels in shellfish on the west coast and highlighted higher

332 toxin concentrations in certain shellfish species, such as the abrupt wedge shell clam
333 (*Donax trunculus*). Conversely our model indicated lower HAB risk associated with
334 harvesting of Pacific oysters or common cockles, with the potential to strategically
335 target the cultivation and collection of alternative species, as we illustrated for the
336 north coast of France (Figure 6).

337

338 Furthermore, using a combination of machine learning and statistical models we
339 have demonstrated previously unseen levels of accuracy when forecasting HAB
340 toxins in shellfish up to 8 weeks into the future, for a geographically diverse set of 6
341 study sites in SW England and Scotland. Our longer-term forecast modelling
342 provides new opportunities for mitigation activities requiring more advanced warning,
343 notably targeting *in situ* end-product testing and informing site-specific harvest
344 scheduling, e.g. directing harvesting activities to alternative locations until toxins
345 have purged (depurated) from shellfish. Crucially for practicality of daily operational
346 use, the computational run time for these algorithms is just a few seconds per site,
347 while requiring very basic CPU, memory, and storage resources.

348

349 The power and wide applicability of our models stems from the integration of
350 substantial (10-20 year) EU-standardised, national shellfish monitoring data. These
351 publicly available data are updated on a weekly (or bi-weekly) basis, which allows for
352 continual model recalibration, assuring the validity of spatial interpolations and short-
353 to long-term future predictions of HAB toxin accumulation in shellfish. While we
354 acknowledge that multi-decadal data are required to discern long-term trends and
355 confirm HAB drivers (causal factors), holding out for extended time-series data (>10-
356 20 years) won't necessarily help anticipate unforeseen future changes. For example,
357 there have been notable increases in the occurrence of HABs following major
358 hydroclimatic regime shifts, such as North Atlantic Oscillation switching abruptly
359 (NAO+) and generating stronger westerly winds and milder, wetter winters since the
360 mid-1980s in the North-East Atlantic and North Sea^{16,30,31}. Here we take the
361 pragmatic approach of constantly updating contemporary signals, as well as
362 reviewing of longer-term signals, based on *Dinophysis* spp. abundance and other
363 readily available proximate predictor variables - here sea surface temperature
364 (obtained daily) - resulting in compelling prediction accuracy.

365

366 3.2 Scope to improve HAB risk assessment and forecasting

367 Predicting low biomass HABs using models is a key priority because their
368 progression is difficult to track by traditional microscopic methods or by high
369 resolution Earth observation systems³². Furthermore, low biomass HAB species
370 including *Dinophysis* spp. can bloom 'under the radar' for protracted periods with
371 limited effects from density-dependent predation, parasitism and competition for
372 resources (compared to high biomass blooms)¹⁵. Nutrient availability is not a major
373 limitation for mixotrophs like *Dinophysis* spp. since they are able to switch between
374 autotrophy (photosynthesis) and heterotrophy (predating other microalgae)^{33,34}.
375 Given the small ecological footprint and trophic plasticity of *Dinophysis* spp., we were
376 able to predict HAB risk with ~87% accuracy (on average) based on histories of only
377 two 'essential' input variables: HAB cell count and sea surface temperature.
378 However, we can foresee situations where more input variables may be needed:
379 i) At sites where availability of HAB cell count data is not available in sufficient
380 quantities, we could include additional variables capturing the conditions that lead to

381 changes in cell abundance, e.g. physical advection, related to wind speed and
382 direction and upwelling^{23,35,36};
383 ii) Other low biomass HAB species might also be predictable from a limited number
384 of variables, but it is likely that accurate prediction of high biomass HABs with larger
385 “ecological footprints” may require a wider range of environmental predictor
386 variables¹⁹;
387 iii) For some HAB species (including both low and high biomass species), cell
388 abundance may not be directly proportional to HAB toxin accumulation in shellfish.
389 This disconnect may occur for example for *Pseudo-nitzschia*, *Alexandrium* and
390 *Prorocentrum* species, and has been attributed to variations in environmental cues
391 stimulating toxin production/release, including temperature, irradiance, nutrient
392 levels, and abundances of predators^{15,18}.
393 iv) Different shellfish species have different propensities for accumulating HAB
394 toxins, which may be exacerbated by variation in site-specific environmental
395 conditions affecting toxin production, as well as uptake and depuration by shellfish
396 e.g. temperature, chlorophyll and turbidity levels, which can affect ventilation,
397 filtration, egestion, metabolic and excretion rates in shellfish^{6,37}.

398
399 Moreover, while we succeeded in separately tackling the aims of spatially quantifying
400 long-term risk from HABs and generating more accurate forecasts of HAB impacts
401 on shellfish quality at relatively data-rich individual sites, future modelling should
402 combine these efforts to generate forecasts for data-poor sites, by pooling
403 information about recent HAB events and the effects of predictor variables across
404 sites. Importantly for achieving this goal and for addressing situations i) to iv), the
405 flexibility and generality of the approaches presented here mean it is very
406 straightforward to include additional inputs. For example, site-specific data, including
407 exposure and water depth, which govern mixing versus stratification, may
408 significantly increase predictive power for several HAB species¹⁵.

409
410 Finally, we acknowledge there are several avenues for improving data collection to
411 benefit HAB risk assessment. First, resolution of *Dinophysis* bloom dynamics could
412 be improved by acquiring real-time data from *in situ* sensors capable of near real-
413 time quantification of changing HAB toxin concentrations and HAB species
414 abundance via cytometric or molecular-based methods³⁸⁻⁴⁰. Prediction of *Dinophysis*
415 toxin concentrations in shellfish could also potentially be improved by discerning cell
416 counts for prominent species, which have different toxin profiles – including
417 *Dinophysis acuminata* and *Dinophysis acuta*, which are most regularly associated
418 with intoxication of bivalve shellfish in key shellfish growing regions from NW
419 Scotland and Scandinavia to the Iberian Peninsula and the Mediterranean^{35,36,41}.

420
421 So far, only a limited number of real-time monitoring systems have been
422 implemented in national or regional HAB surveillance programmes: NOAA’s HAB
423 operational forecast system for the Gulf of Mexico^{42,43}; the Autonomous Ocean
424 Sampling Network including Monterey Bay⁴⁴, the Gulf of Maine⁴⁵, and the Hong
425 Kong coast⁴⁶. There is huge scope to expand and advance HAB monitoring systems,
426 but this work should be undertaken in tandem with the advancement of data-driven
427 models that can help direct data acquisition to where this is most needed (i.e. HAB
428 hotspots) and to ultimately exploit these data in terms of HAB risk forecasting.

429 4 Supplementary Information

430

431 Spreadsheet **Data Summary.xlsx** quantifies the extent of the phycotoxin data used
432 in this analysis and spreadsheet **Performance.xlsx** contains all predictive
433 performance metrics for the 6 trial sites (as detailed in Sections 2.2 and 5.2). Plots of
434 smoothed temperature and *Dinophysis* abundance input variables are
435 (**Smoothed.pdf**) and plots of raw and corrected predictions for the 6 trial sites
436 (**Predictions.pdf**) are provided for download. Finally, all code and data used in this
437 analysis are provided for download in a single ZIP file **Code and Data.zip**.

438 5 Methods

439

440 Standardised HAB monitoring data used in this analysis span 12 years (2008-2020)
441 and include a total of 302 sites and at least 19 shellfish species farmed or collected
442 in Scotland, SW England and Northern France (Data Summary). At routine
443 monitoring points for each of these sites, HAB toxins are measured in shellfish meat
444 each week during blooms, in conjunction with measurements of HAB species
445 abundance according to official control methods stipulated in EU Hygiene Regulation
446 (EC) No 853/2004 (EC, 2004). In the following subsections we leverage this data to
447 develop models for assessing the long-term risks of HABs (Section 5.1) and models
448 for nowcasting and forecasting toxin concentration, in combination with temperature
449 data and *Dinophysis* spp. abundance data (Section 5.2).

450

451 5.1 Spatiotemporal risk assessment models

452 For assessment of long-term average toxin levels from HABs, we have developed
453 statistical/probabilistic models within the Generalized Additive Model²⁷ (GAM)
454 framework. First, we assume that toxin samples y can be modelled using a log-
455 Normal distribution (i.e. $\log(y) \sim \text{Normal}(\mu, \sigma^2)$). We can then characterise
456 systematic variability in average toxin levels by including spatio-temporal structures
457 and other important variables in the mean of this distribution. These structures are
458 defined as linear combinations of basis functions, typically smooth spline functions of
459 one or more variables. The functions are estimated under a smoothness constraint
460 to prevent overfitting, which is optimised using a measure of out-of-sample predictive
461 power. Analysis is based on the estimated functions and associated measures of
462 uncertainty (e.g. 95% confidence intervals), and predictions are based on estimates
463 of μ .

464

465 The power of the GAM framework for this application is that by specifying functions
466 of time and space (longitude and latitude) in the model we can account for
467 spatiotemporal variation in phycotoxin levels. For instance, seasonal cycles in HAB
468 occurrence may vary substantially over a large geographical region, or the risk from
469 HABs may increase or decrease at different locations due to changes in ocean
470 regimes or climate. Taking these spatiotemporal structures into account can better
471 inform decisions about geographical expansion/diversification of mariculture.
472 Specifically, we can more reliably estimate HAB risk at data-poor sites because: a)
473 the model is more parametrically constrained compared to models where temporal
474 variability is assumed independent for each site; and b) it is possible for data-poor
475 sites to borrow information on HAB risk from nearby data-rich sites.

476

477 For a toxin measurement $y_{t,s,i,j}$ observed on day $t = 1, \dots, N$ (with day in the year $d =$
478 $1, \dots, 365$), at geographical location $s \in S$, in species i (e.g. mussels, oysters) and in
479 production\harvesting area $j = 1, \dots, J$, our spatial risk model is given by:

$$\begin{aligned} 481 \quad & \log(y_{t,s,i,j}) \sim \text{Normal}(\mu_{t,s,i,j}, \sigma_y^2) \\ 482 \quad & \mu_{t,s,i,j} = \text{intercept} + \text{species} + f_1(\text{time}) + f_2(\text{season}) + f_3(\text{space}) + f_4(\text{space, season}) \\ 483 \quad & \quad \quad \quad + f_5(\text{space, time}) \end{aligned}$$

485 First, the species factor effect captures overall differences in the uptake of HAB
486 toxins by different shellfish species, with blue mussels acting as the baseline
487 (intercept) species for all regions (Figure 5). Then, $f_1(\text{time})$ is the overall temporal
488 trend (Figure 3a) for the region of interest, intended to capture the overall inter- and
489 intra-annual signal for each study region. For example, it is this function we could
490 examine for any possible evidence of long-term trends in HAB intensity associated
491 with climate change. Here we define $f_1(\text{time})$ as a thin-plate spline of time (in days)
492 with 50 knots spread evenly across the time series, which is more than adequate to
493 capture general ‘good’ and ‘bad’ periods, as well as longer term trends. The specific
494 basis representation chosen imitates a 1D Gaussian process with a Matérn
495 covariance function^{27,47}. The next function $f_2(\text{season})$ is the overall ‘seasonal’ signal
496 (Figure Figure 3b), i.e. what happens on average in the region depending on the
497 time of year. This is intended to capture the average timing and intensity of HABs in
498 the calendar year. We define $f_2(\text{season})$ as a cyclic cubic spline of calendar day
499 (cyclic means the value is the same for day 0 and day 365), with 10 knots spread
500 evenly across the calendar year. Spatial effect $f_3(\text{space})$ is specified as a 2D thin-
501 plate spline of longitude and latitude. The specific basis representation imitates a 2D
502 Gaussian process in space with an isotropic Exponential function covariance
503 function²⁷. For this function, we specified varying numbers of knots for SW England
504 (50), Scotland (100) and France (100), reflecting differences in spatial extent. It is
505 this function we examine in Figure 1 and Figure 2 to draw conclusions about the
506 geographical distribution of HAB risk.

507
508 In the GAM framework it is possible to capture nonlinear interactions between 2 or
509 more variables. One option is to specify isotropic smooth functions (i.e. the
510 smoothness is invariant to rotation of the coordinate axes²⁷), however this isotropy
511 may be inappropriate for interactions involving variables with very different scales
512 e.g. space and time. A section option which we will use here is to use tensor
513 products which interacts smooths across multiple variables⁴⁸, resulting in different
514 smoothness penalties for each dimension. First, $f_4(\text{space, season})$ interacts a 2D thin
515 plate spline (50 knots for France and Scotland, 25 for SW England) of latitude and
516 longitude with a 1D cubic cyclic spline of calendar day (10 knots), resulting in a 3D
517 function which captures spatial variability in the seasonal signal (e.g. Figure 4).
518 Similarly, $f_5(\text{space, time})$ combines a 2D thin-plate spline of longitude and latitude (10
519 knots) with a 1D thin-plate spline (10 knots) of time (days), to capture spatial
520 variability in long-term temporal trends.

521
522 To assess the relative importance of the different functions/effects, we can
523 decompose fitted values μ into each term and compute the percentage of the
524 variance of the toxin measurements y explained by each term. For France, the most
525 important term was the spatial function f_3 (22%), followed by the species effect

526 (16%) – reflecting the wide variety of species being cultivated in France – and the
527 space-season interaction f_4 (12%). In SW England, the spatial function f_3 was also
528 most important (19%), followed by the function of time f_1 (16%) – reflecting the
529 significant interannual variability for SW England as seen in Figure 3 – followed by
530 the space-season interaction f_4 (15%). Finally, in Scotland the spatial and space-
531 season terms were tied as the most important (19% each), followed by the seasonal
532 function f_2 (17%).
533

534 5.2 Nowcasting and forecasting

535 The general concept of our approach to nowcasting and forecasting is to model
536 *Dinophysis* toxicity in shellfish tissue as an estimated function of two inputs: sea
537 surface temperature and *Dinophysis* spp. abundance (total cell counts measured per
538 litre of seawater). The daily averaged surface sea temperature was extracted from
539 the Copernicus Marine Environment Monitoring Service reanalysis ocean product
540 NWSHELF_MULTIYEAR_PHY_004_009 version 5 produced by the UK Met Office.
541 The system is the Forecasting Ocean Assimilation Model 7 km Atlantic Margin model
542 (FOAM AMM7), based on version 3.6 of the Nucleus for European Modelling of the
543 Ocean (NEMO) ocean model code⁴⁹. The model domain resolves all shelf seas
544 surrounding the UK and includes all the sites considered here at 7km resolution in
545 the horizontal and with the vertical dimension discretised into 51 vertical layers. The
546 reanalysis includes daily assimilation of satellite derived sea surface temperature
547 (SST) and profiles of temperature and salinity assimilated using version 6 of
548 NEMOVar⁵⁰. For each shellfish site, daily temperature values were extracted for the
549 nearest grid cell for which temperature data is available.
550

551 The 3 Scottish trial sites (Loch Eishort, Loch Laxford and Sandsound Voe) were
552 selected by first quantifying data availability for all sites by ranking the product of the
553 number of toxin samples and the number of abundance samples, and then selecting
554 the 3 sites with the highest data availability. The 3 trial sites in SW England were
555 selected by considering both data availability and diversity of site location and type
556 (i.e. offshore vs coastal vs estuarine). For nowcasting and forecasting, all sites were
557 modelled separately, so the remainder of this section details the approach for an
558 individual site.
559

560 Both short-term and long-term histories of sea surface temperature and abundance
561 have the potential to be informative. However, linking toxin observations with
562 previous *Dinophysis* cell counts is challenging due to large gaps and significant
563 noise in the time series of abundance measurements. To tackle both issues, we fit
564 the (log) abundance values using a simple Generalized Additive Model²⁷, consisting
565 of smooth functions of time and time of year. The same approach is applied to the
566 temperature values to smooth out any short-term “spikiness”, which was occasionally
567 exploited by some models to overfit the data. This results in continuous “smooth”
568 time series of temperature and abundance, which do not strictly interpolate the
569 observed values but instead aim to reflect the underlying “average” trend (reference
570 supporting information). Starting 12 weeks after the earliest abundance
571 observations, we then create lagged versions of the smoothed temperature and
572 abundance variables, with the lag increasing up to 12 weeks in steps of 1 week. For
573 example, the 2-week lagged temperature variable is equal to the value of the
574 smoothed temperature variable 2 weeks ago. The result of this procedure is 13
575 temperature variables and 13 abundance variables.

576

577 To accurately predict toxin values using (up to) all 26 of these variables as inputs, we
578 require a modelling framework which can account for complex interactions between
579 inputs. One example of a possible interaction effect is if the differences between the
580 lagged abundance variables can predict the rate of change in the toxin. Random
581 forests are a very straightforward option to achieve capture complex interactions,
582 while also being robust to correlated inputs of potentially different scales. Random
583 forests optimally discretise the multi-dimensional space of the inputs, into contiguous
584 “regions” where the predicted quantity is homogeneous. In its most basic form, it can
585 be thought of as a moving window approach, albeit a robust one by being applied to
586 different subsamples of the data. To fit random forests in R using the *ranger*⁵¹
587 package, we need only specify the output variable, here the logarithm of the toxin
588 values, and the inputs, here the lagged variables. There is no need to specify any
589 interactions when defining the model. The only argument we modified was the
590 number of trees, which we increased from 500 to 1000, which has the effect of
591 slightly decreasing the error of the random forest at the expense of computation
592 time.

593

594 When making future predictions we must consider that future values of abundance
595 and temperature (where site-specific forecasts of sea surface temperature are
596 unavailable) will be unknown. Specifically, values of our lagged variables for lags
597 less than the forecasting lead time will be unknown. Therefore, the forecasting
598 experiment presented in Section 2 was constructed by specifying distinct random
599 forest models for each lead time, where each model includes only lagged variables
600 which would be observed for that lead time. We specified models with a lead time of
601 0 weeks (nowcasting), 1 week, 2 weeks, 4 weeks, 6 weeks, and 8 weeks. A final
602 model was fit with all lags treated as observed, to investigate how well the model
603 might be able to predict toxicity if accurate forecasts of abundance and temperature
604 were available. These models are implemented in a loop to generate predictions for
605 the last 80 toxin observations in the time series.

606

607 Out-of-sample prediction errors (defined as the observed value minus the prediction)
608 for each lead time are stored as the prediction experiment progresses through the
609 time series. Using a further Generalized Additive Model with a spline function of time
610 to be estimated (one knot for every 2 observations), we can model the errors to
611 estimate any short-term systematic bias in the forecasts. Then, we can predict the
612 error of the next forecast and add together the predicted error and the predicted toxin
613 value, to obtain a “corrected” prediction. This approach is similar to how statistical
614 post-processing methods are used to correct numerical weather predictions. Again,
615 we consider the lead time, so we only provide the GAM with errors which would be
616 known when making the next prediction. The post-processing model is only
617 implemented after at least 20 predictions have been made by the machine learning
618 algorithm, so that enough data is available to begin predicting new errors. Finally, we
619 compute a basic measure of out-of-sample uncertainty by calculating the sample
620 standard deviation of the new errors, defined as the observed value minus the
621 corrected prediction.

622

623 5.3 Handling of missing values

624 For the French phycotoxin data, we assume that the entire distribution of toxin
625 concentrations has been observed, noting that around half of measurements are low

626 values in the single figures. In both the UK phycotoxin datasets, particularly for SW
627 England, a high proportion of observations were recorded as '<RL' – around 80% of
628 the Scottish data and around 90% of the SW English data – meaning the toxin
629 concentration was too low to be detected. Nonetheless, these observations can
630 provide valuable information on the periods of the time and locations where the toxin
631 level was low. To accommodate such data in our spatiotemporal models for SW
632 England and Scotland, as well as in our forecasting models for sites in SW England,
633 we replaced all <RL entries with a fixed value below the lowest measured value, 10
634 µg/kg OA. For the Scottish 3 Scottish trial sites (Loch Eishort, Loch Laxford and
635 Sandsound Voe), on the other hand, we obtained the best forecasting performance
636 when all '<RL' observations were discarded. Prediction performance metrics RMSE
637 and R² were calculated using only detected concentrations. All other missing values
638 were discarded.

639
640 For the Scottish *Dinophysis* spp. abundance data, we discarded values equal to 0.
641 For the SW English *Dinophysis* spp. abundance data, we replaced values below the
642 detection threshold (recorded as 'ND') with a fixed value below the lowest measured
643 value, which we chose to be 20 cells per litre. All other missing values were
644 discarded.

645 Author Contributions

646 Stoner undertook data-driven modelling and preparation of the manuscript. The
647 following authors also contributed to the manuscript: Economou provided expert
648 input on the study and statistical framework design; Ashton, Torres and Brown
649 provided expert input on climatic, oceanographic, and biogeochemical covariates.
650 Brown conceived and coordinated the study.

651 Competing Interests

652 The authors declare no competing interests.

653 Acknowledgements

654 The authors gratefully acknowledge funding from the European Maritime and
655 Fisheries Fund (ENG3103); Turing Pilot Research Grant (260320) and IIB Open
656 Innovation Project Fund (115717).

- 657
658 1 Food and Agriculture Organization. The State of World Fisheries and Aquaculture
659 2020. Sustainability in action. (Rome, 2020).
- 660 2 Costello, C. *et al.* The future of food from the sea. *Nature* **588**, 95-100,
661 doi:10.1038/s41586-020-2616-y (2020).
- 662 3 van der Schatte Olivier, A. *et al.* A global review of the ecosystem services provided
663 by bivalve aquaculture. *Reviews in Aquaculture* **12**, 3-25,
664 doi:<https://doi.org/10.1111/raq.12301> (2020).
- 665 4 Daniels, C. *et al.* Supporting Mariculture Development: Evidence for Informed
666 Regulation. Policy Brief. (2020).
- 667 5 Ferreira, J. G. *et al.* Analysis of coastal and offshore aquaculture: Application of the
668 FARM model to multiple systems and shellfish species. *Aquaculture* **292**, 129-138,
669 doi:<https://doi.org/10.1016/j.aquaculture.2009.03.039> (2009).

- 670 6 Brown, A. R. *et al.* Assessing risks and mitigating impacts of harmful algal blooms on
671 mariculture and marine fisheries. *Reviews in Aquaculture* **12**, 1663-1688,
672 doi:<https://doi.org/10.1111/raq.12403> (2020).
- 673 7 Glibert, P. M. *et al.* Vulnerability of coastal ecosystems to changes in harmful algal
674 bloom distribution in response to climate change: projections based on model
675 analysis. *Global Change Biology* **20**, 3845-3858,
676 doi:<https://doi.org/10.1111/gcb.12662> (2014).
- 677 8 Weisberg, R. H. *et al.* The Coastal Ocean Circulation Influence on the 2018 West
678 Florida Shelf K. brevis Red Tide Bloom. *Journal of Geophysical Research: Oceans* **124**,
679 2501-2512, doi:<https://doi.org/10.1029/2018JC014887> (2019).
- 680 9 Trainer, V. L. *et al.* GlobalHAB: Evaluating, reducing and mitigating the cost of
681 Harmful Algal Blooms: A Compendium of case studies. *PICES Press* **28**, 30-32 (2020).
- 682 10 Wells, M. L. *et al.* Future HAB science: Directions and challenges in a changing
683 climate. *Harmful Algae* **91**, 101632, doi:<https://doi.org/10.1016/j.hal.2019.101632>
684 (2020).
- 685 11 Joint Group of Experts on the Scientific Aspects of Marine Environmental Protection
686 (GESAMP). Protecting the Oceans from Land-based Activities: Land-based sources
687 and activities affecting the quality and uses of the marine, coastal and associated
688 freshwater environment., (2001).
- 689 12 Berdalet, E. *et al.* Marine harmful algal blooms, human health and wellbeing:
690 challenges and opportunities in the 21st century. *Journal of the Marine Biological*
691 *Association of the United Kingdom* **96**, 61-91, doi:10.1017/S0025315415001733
692 (2016).
- 693 13 Reguera, B. *et al.* Dinophysis Toxins: Causative Organisms, Distribution and Fate in
694 Shellfish. *Marine Drugs* **12**, 394-461 (2014).
- 695 14 Manfrin, C. *et al.* Physiological and molecular responses of bivalves to toxic
696 dinoflagellates. *Invertebrate Survival Journal* **9** (2012).
- 697 15 Wells, M. L. *et al.* Harmful algal blooms and climate change: Learning from the past
698 and present to forecast the future. *Harmful Algae* **49**, 68-93,
699 doi:<https://doi.org/10.1016/j.hal.2015.07.009> (2015).
- 700 16 Gobler, C. J. *et al.* Ocean warming since 1982 has expanded the niche of toxic algal
701 blooms in the North Atlantic and North Pacific oceans. *Proceedings of the National*
702 *Academy of Sciences* **114**, 4975, doi:10.1073/pnas.1619575114 (2017).
- 703 17 European Union. (Official Journal of the European Union, 2004).
- 704 18 Anderson, D. M., Cembella, A. D. & Hallegraeff, G. M. Progress in Understanding
705 Harmful Algal Blooms: Paradigm Shifts and New Technologies for Research,
706 Monitoring, and Management. *Annual Review of Marine Science* **4**, 143-176,
707 doi:10.1146/annurev-marine-120308-081121 (2011).
- 708 19 Davidson, K. *et al.* Forecasting the risk of harmful algal blooms. *Harmful algae* **53**, 1-
709 7, doi:10.1016/j.hal.2015.11.005 (2016).
- 710 20 Gillibrand, P. A., Siemering, B., Miller, P. I. & Davidson, K. Individual-based modelling
711 of the development and transport of a *Karenia mikimotoi* bloom on the North-west
712 European continental shelf. *Harmful Algae* **53**, 118-134,
713 doi:<https://doi.org/10.1016/j.hal.2015.11.011> (2016).
- 714 21 Karasiewicz, S., Chapelle, A., Bacher, C. & Soudant, D. Harmful algae niche responses
715 to environmental and community variation along the French coast. *Harmful Algae*
716 **93**, 101785, doi:<https://doi.org/10.1016/j.hal.2020.101785> (2020).

- 717 22 Janssen, A. B. G. *et al.* How to model algal blooms in any lake on earth. *Current*
718 *Opinion in Environmental Sustainability* **36**, 1-10,
719 doi:<https://doi.org/10.1016/j.cosust.2018.09.001> (2019).
- 720 23 Schmidt, W. *et al.* A generic approach for the development of short-term predictions
721 of *Escherichia coli* and biotoxins in shellfish. *Aquac Environ Interact* **10**, 173-185,
722 doi:10.3354/aei00265 (2018).
- 723 24 Taranu, Z. E., Gregory-Eaves, I., Steele, R. J., Beaulieu, M. & Legendre, P. Predicting
724 microcystin concentrations in lakes and reservoirs at a continental scale: A new
725 framework for modelling an important health risk factor. *Global Ecology and*
726 *Biogeography* **26**, 625-637, doi:<https://doi.org/10.1111/geb.12569> (2017).
- 727 25 Cusack, C. *et al.* Harmful algal bloom forecast system for SW Ireland. Part II: Are
728 operational oceanographic models useful in a HAB warning system. *Harmful Algae*
729 **53**, 86-101, doi:<https://doi.org/10.1016/j.hal.2015.11.013> (2016).
- 730 26 Davidson, K. *et al.* HABreports: Online Early Warning of Harmful Algal and Biotoxin
731 Risk for the Scottish Shellfish and Finfish Aquaculture Industries. *Frontiers in Marine*
732 *Science* **8**, doi:10.3389/fmars.2021.631732 (2021).
- 733 27 Wood, S. N. *Generalized Additive Models: An Introduction with R, Second Edition.*
734 (CRC Press, 2017).
- 735 28 Pingree, R. D., Pugh, P. R., Holligan, P. M. & Forster, G. R. Summer phytoplankton
736 blooms and red tides along tidal fronts in the approaches to the English Channel.
737 *Nature* **258**, 672-677, doi:10.1038/258672a0 (1975).
- 738 29 Pingree, R. D., Mardell, G. T. & Maddock, L. A marginal front in Lyme Bay. *Journal of*
739 *the Marine Biological Association of the United Kingdom* **63**, 9-15,
740 doi:10.1017/S0025315400049754 (1983).
- 741 30 Drouard, M., Kornhuber, K. & Woollings, T. Disentangling Dynamic Contributions to
742 Summer 2018 Anomalous Weather Over Europe. *Geophysical Research Letters* **46**,
743 12537-12546, doi:<https://doi.org/10.1029/2019GL084601> (2019).
- 744 31 Raine, R., Edwards, M., Reid, P., Bresnan, E. & Fernand, L. Harmful Algal Blooms in
745 Marine Climate Change Impacts Annual Report Card 2007–2008. (2008).
- 746 32 Caballero, I., Fernández, R., Escalante, O. M., Mamán, L. & Navarro, G. New
747 capabilities of Sentinel-2A/B satellites combined with in situ data for monitoring
748 small harmful algal blooms in complex coastal waters. *Scientific Reports* **10**, 8743,
749 doi:10.1038/s41598-020-65600-1 (2020).
- 750 33 Park, M. *et al.* First successful culture of the marine dinoflagellate *Dinophysis*
751 *acuminata*. *Aquatic Microbial Ecology* **45**, 101-106 (2006).
- 752 34 Flynn, K. J. & McGillicuddy, D. J. in *Harmful Algal Blooms* 115-134 (2018).
- 753 35 Díaz, P. A. *et al.* Mesoscale Dynamics and Niche Segregation of Two *Dinophysis*
754 Species in Galician-Portuguese Coastal Waters. *Toxins* **11**, 37 (2019).
- 755 36 Fernández, R. *et al.* *Dinophysis* Species and Diarrhetic Shellfish Toxins: 20 Years of
756 Monitoring Program in Andalusia, South of Spain. *Toxins* **11**, 189 (2019).
- 757 37 Basti, L. *et al.* Harmful algal blooms and shellfish aquaculture in changing
758 environment. *Bulletin of Japan Fisheries Research and Education Agency* (2019).
- 759 38 Bickman, S. R. *et al.* An Innovative Portable Biosensor System for the Rapid Detection
760 of Freshwater Cyanobacterial Algal Bloom Toxins. *Environmental Science &*
761 *Technology* **52**, 11691-11698, doi:10.1021/acs.est.8b02769 (2018).

762 39 Scholin, C. *et al.* The Quest to Develop Ecogenomic Sensors: A 25-Year History of the
763 Environmental Sample Processor (ESP) as a Case Study. *Oceanography* **30**, 100-113,
764 doi:<https://doi.org/10.5670/oceanog.2017.427> (2018).

765 40 McPartlin, D. A. *et al.* Biosensors for the monitoring of harmful algal blooms. *Current*
766 *Opinion in Biotechnology* **45**, 164-169,
767 doi:<https://doi.org/10.1016/j.copbio.2017.02.018> (2017).

768 41 Swan, S. C. *et al.* Dinophysis acuta in Scottish Coastal Waters and Its Influence on
769 Diarrhetic Shellfish Toxin Profiles. *Toxins* **10**, 399, doi:10.3390/toxins10100399
770 (2018).

771 42 Campbell, L., Henrichs, D. W., Olson, R. J. & Sosik, H. M. Continuous automated
772 imaging-in-flow cytometry for detection and early warning of *Karenia brevis* blooms
773 in the Gulf of Mexico. *Environ Sci Pollut Res Int* **20**, 6896-6902, doi:10.1007/s11356-
774 012-1437-4 (2013).

775 43 National Oceanographic and Atmospheric Administration. *Gulf of Mexico Harmful*
776 *Algal Bloom Forecast, Tides and Currents*,
777 <<https://tidesandcurrents.noaa.gov/hab/gomx.html>> (2021).

778 44 Thompson, A. *et al.* Satellites to seafloor: Toward fully autonomous ocean sampling.
779 *Oceanography* **30**, 160-168 (2017).

780 45 Anderson, C. R. *et al.* Scaling Up From Regional Case Studies to a Global Harmful
781 Algal Bloom Observing System. *Frontiers in Marine Science* **6**,
782 doi:10.3389/fmars.2019.00250 (2019).

783 46 Yamahara, K. M. *et al.* In situ Autonomous Acquisition and Preservation of Marine
784 Environmental DNA Using an Autonomous Underwater Vehicle. *Frontiers in Marine*
785 *Science* **6**, doi:10.3389/fmars.2019.00373 (2019).

786 47 Kammann, E. E. & Wand, M. P. Geoadditive models. *Journal of the Royal Statistical*
787 *Society: Series C (Applied Statistics)* **52**, 1-18, doi:[https://doi.org/10.1111/1467-](https://doi.org/10.1111/1467-9876.00385)
788 [9876.00385](https://doi.org/10.1111/1467-9876.00385) (2003).

789 48 Wood, S. N. Low-Rank Scale-Invariant Tensor Product Smooths for Generalized
790 Additive Mixed Models. *Biometrics* **62**, 1025-1036, doi:10.1111/j.1541-
791 0420.2006.00574.x (2006).

792 49 NEMO Ocean Engine (Zenodo, 2019).

793 50 Kristian, M. & M. Alonso Balmaseda, A. W. (ECMWF, 2012).

794 51 Wright, M. N. & Ziegler, A. ranger: A Fast Implementation of Random Forests for
795 High Dimensional Data in C++ and R. *2017* **77**, 17, doi:10.18637/jss.v077.i01 (2017).
796

Supplementary Files

This is a list of supplementary files associated with this preprint. Click to download.

- [DataSummary.xlsx](#)
- [Performance.xlsx](#)
- [Predictions.pdf](#)
- [Smoothed.pdf](#)